Applied Catalysis B: Environmental 241 (2019) 120–129

Contents lists available at ScienceDirect

Applied Catalysis B: Environmental

journal homepage: www.elsevier.com/locate/apcatb

Dechlorination of triclosan by enhanced atomic hydrogen-mediated electrochemical reduction: Kinetics, mechanism, and toxicity assessment

Ran Mao[a], Chao Huang[a], Xu Zhao[a,b,*], Mei Ma[a], Jiuhui Qu[a]

[a] Key Laboratory of Drinking Water Science and Technology, Research Center for Eco-Environmental Sciences, Chinese Academy of Sciences, Beijing, 100085, PR China
[b] University of Chinese Academy of Sciences, Beijing, 100049, PR China

ARTICLE INFO

Keywords:
Electrochemical dechlorination
Halogenated organic compounds
Atomic hydrogen
Indirect reduction

ABSTRACT

Environmental-friendly and efficient technologies for the removal of halogenated organic compounds in water are highly desired. Triclosan (TCS) is a potential threat to the environment and human health, and is resistant to biodegradation. Here, a Pd/N-GR/Cu foam exhibits a much enhanced activity as the cathode for TCS degradation by electrochemical reduction. The dechlorination rate of Pd/N-GR/Cu foam is 5.50, 6.49, and 14.68 times higher than Pd/Cu, N-GR/Cu, and Cu foam, respectively. The leaching of Pd and Cu is inhibited due to the protection by cathodic currents and alkaline conditions. 2- and 1-chlorinated isomers are the main intermediates, and the final products are completely dechlorinated 2-phenoxyphenol with a small amount of further H radical addition product 6-phenoxycyclohex-3-enol. ESR spin trapping results indicate the coupling of Pd and N-GR promotes the production and utilization of atomic H*, and the contribution of atomic H* obeys the order of Pd/N-GR/Cu (68.5%) > Pd/Cu (56.6%) > N-GR/Cu (24.3%) > Cu (5.7%). The bacterial cytotoxicity and AhR activity of TCS solution after 60 min are decreased by 83.2% and 90.3%, respectively. The electrochemical reduction can be a promising option for supplementing the current technologies for TCS abatement in wastewater.

1. Introduction

First used in the early 1970s as a component of surgical hand scrub agent, triclosan (5-chloro-2-(2,4-dichlorophenoxy)phenol, TCS) is a pervasive antimicrobial disinfectant which has been extensively used in pharmaceutical and personal care products [1,2]. Excess utilization of TCS results in its ubiquitous presence in the environment [3]. In addition to its high toxicity to bacteria, TCS also has adverse effects on aquatic organisms (eg. chronical and acute toxicity, and endocrine disrupting effect) [4,5]. Various treatment technologies for the removal of TCS from water have been investigated, including nanofiltration, potassium permanganate oxidation, ozonation, Fenton and electro-Fenton oxidation, anodic oxidation, photolysis, and thermally activated persulfate oxidation [6–15].

Meanwhile, the electrochemical reductive treatment for the halogenated organics abatement is drawing increasing concern because of its high efficiency and efficient minimization of chemicals and secondary pollution [16–19]. For example, Durante et al. realized the effective dehalogenation of polychloromethanes at silver and carbon electrodes by electrochemical reduction [20], while Huang et al. demonstrated the reductive removal of trichloroacetic acid by a flow-through electrode consisted of the cobalt doped MoS_2 catalyst and carbon felt substrate [21]. As the toxicity of halogenated organic compounds (HOCs) is mainly caused by the C—X bonds (X are halogen atoms) in the molecular structure, the electrochemical reduction enables the selective breakage of C—X bonds, thereby mitigating the toxic effects of HOCs.

The direct reduction by cathode electrons and indirect atomic H* reduction are two generally accepted avenues for the electrochemical reduction [22]. The efficient production and utilization of active atomic H* (E° = −2.1 V vs RHE) is considered to be the key to improve the treatment efficiency and lower the energy cost [23]. Since Pd owns a high capacity of adsorption and reserve of atomic H*, it has been considered an ideal catalyst for electrocatalytic dehalogenation [24,25]. Three-dimensional graphene (3D GR) support, owing to its high surface area and electrical conductivity, has been frequently employed for the enhancement of metal catalysts in electrochemical applications [26]. Doping with heteroatoms such as nitrogen (N), boron (B), and sulfur (S) can further modify its electronic properties. For example, N can interact with carbons and donate electrons into GR's

* Corresponding author at: Key Laboratory of Drinking Water Science and Technology, Research Center for Eco-Environmental Sciences, Chinese Academy of Sciences, Beijing, 100085, PR China.
E-mail address: zhaoxu@rcees.ac.cn (X. Zhao).

https://doi.org/10.1016/j.apcatb.2018.09.013
Received 22 June 2018; Received in revised form 30 August 2018; Accepted 4 September 2018
Available online 08 September 2018
0926-3373/

substrate, resulting in improved conductivities and charge transfer [27]. The incorporated N atoms also enabled activating of adjacent C atoms in C—N groups. However, the previous studies pertaining to the N-doped 3D GR supported Pd catalysts primarily focused on the oxygen reduction reactions, fuel cells, electrochemical sensors, and energy storage [28–31]. To the best of our knowledge, no investigations of this material in HOCs treatment by electrochemical reduction have been reported, and little is known about the electroreductive degradation of TCS.

In this study, the 3D N-GR was prepared through chemical vapour deposition (CVD) method on the Cu foam substrate, followed by electrodepositing Pd particles to fabricate Pd/N-GR/Cu foam electrode, which was employed for the electrochemical dechlorination of TCS. The objective is to enhance the charge transfer at the electrode interface and promote the production and usage of atomic H* for effective TCS reduction. Our findings indicate that TCS can be completely degraded by the electrocatalytic reduction. The atomic H* mediated indirect reduction process is highly active for the selective cleavage of the C—Cl bonds in TCS molecule, with 2-phenoxyphenol being the major final product. In addition, the toxicity of the TCS solution after electrochemical reduction treatment is evaluated herein.

2. Experimental

2.1. Synthesis of electrodes

N-doped GR was grown on a Cu foam by CVD method in a quartz furnace. Firstly, Cu foam was cleaned in ethanoic acid, ethanol and acetone by ultrasound, and put in the furnace reactor. The reactor was heated to 960 °C at 10 °C/min with the mixed gas of H_2 (35 sccm) and Ar (260 sccm). After 15 min anneal, injection of pyridine vapour into the reactor was conducted through evaporating for 3 min for N-GR deposition. The deposition time of 3 min was chosen because this value was suitable for the N-GR formation with a proper number of layers. A longer deposition time would lead to the increase of the number of N-GR layers and thus a decreased electrical conductivity of N-GR. After that, pyridine vapour was cut off. The N-GR/Cu foam was acquired and used for depositing Pd particles according to the electrodeposition method [32].

2.2. Electrochemical reduction experiments

Electrochemical reduction of TCS was conducted in a cell comprised of two compartments (separated by Nafion-117 membrane), containing a working electrode (superficial area of 10 cm^2), a saturated calomel electrode (SCE, reference electrode), and a Pt wire counter electrode. The anode and cathode distance was ca. 2 cm. The solution volume of both anode and cathode cell was 50 mL. 2 mM Na_2SO_4 was employed for both anolyte and catholyte. Electrochemical experiments were performed in a potentiostatic mode at room temperature (20 ± 1 °C). The initial pH of reaction solution was ca. 9.4 (TCS stock solution was prepared in 1 mM NaOH solution). The cathode cell was magnetically stirred during electrolysis.

2.3. Analytical method

TCS concentration was quantified using a HPLC system (Agilent 1100) with an UV detector of 230 nm A methanol/water mixture (90/10, v/v) was selected as the mobile phase, with the flow rate of 1.0 mL/min and injection volume of 20 μL. Intermediate products were identified by a LC–MS using a high resolution hybrid quadrupole time-of-flight mass spectrometer (LC-Q-TOF-MS, Agilent 6540, USA). The electrospray ion source temperature was 350 °C, and the ion spray voltage was −4000 V. The Chromatographic procedures was conducted according to the method by Chen et al [7].

The concentrations of Cu^{2+} and Pd^{2+} were measured by the inductively coupled plasma/mass spectrometry (ICP/MS). The electron spin resonance (ESR) signals of radicals trapped by 5,5′-dimethyl-1-pirroline-*N*-oxide (DMPO) were examined by a JES-200 ESR spectrometer.

2.4. Electrode characterization

The morphology, structure and surface composition of the electrodes were analyzed by X-ray diffraction (XRD, X'Pert PRO MPD), scanning electron microscope (SEM, JSM-7000 F) equipped with an energy-dispersive X-ray spectrometer (EDS), high-resolution transmission electron microscope (HRTEM, JEOL-2010) coupled with selected-area electron diffraction (SAED), Raman spectroscopy (532 nm laser, Bruker Senterra), and X-ray photoelectron spectroscopy (XPS, ESCALab220I-XL). Electrical impedance spectroscopy (EIS) data was acquired at frequencies from 0.1 to 100 kHz.

2.5. Toxicity assay

Toxicity of the TCS solution during electrochemical reduction were determined by acute toxicity in luminescent bacteria and aryl hydrocarbon receptor (AhR) activity by ethoxyresorufin *O*-deethylase (EROD) assay. Section S1 in SI presents the details of methods for acute toxicity test with Q67 and EROD assay with rat hepatoma (H4IIE) cells.

3. Results and discussion

3.1. Characterization of electrodes

XRD analysis of Cu foam, N-GR/Cu foam, and Pd/N-GR/Cu foam with various Pd loadings are recorded in Fig. 1. Similar metallic Cu planes can be detected for all electrodes. The synthesis of N-GR did not change the structure of the Cu foam substrate. Upon Pd loading, the XRD patterns show the predominance of the (111) plane of Pd, while the (200) and (220) peak is hardly seen. With the decrease of the Pd loading, the (111) plane of Pd diminished as the surface Pd concentration decreased.

The SEM image of Cu foam exhibits a typical scaffold architecture and smooth surface with clear zigzag lines (Fig. 2a). On the Cu foam surface, the Pd particles are spherical aggregates composed of smaller grains of ~30 nm (Fig. 2b). While on N-GR/Cu foam, dense irregular Pd cuboids with squamose structure can be clearly identified (Fig. 2c). EDS results show the relatively uniform distribution of the Pd particles and N-GR sheets (Fig. 2d). HRTEM image of N-GR in Fig. 3a presents a multilayered structure of graphite layers, and the corresponding SAED

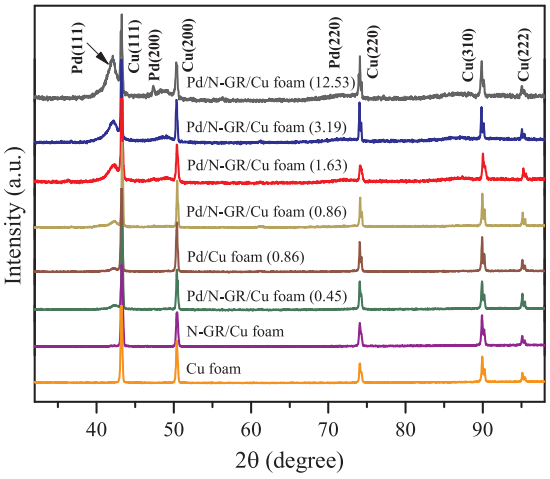

Fig. 1. XRD patterns of Cu foam, N-GR/Cu foam, and Pd/N-GR/Cu foam with various Pd loadings (mg cm^{-2}, marked with parentheses).

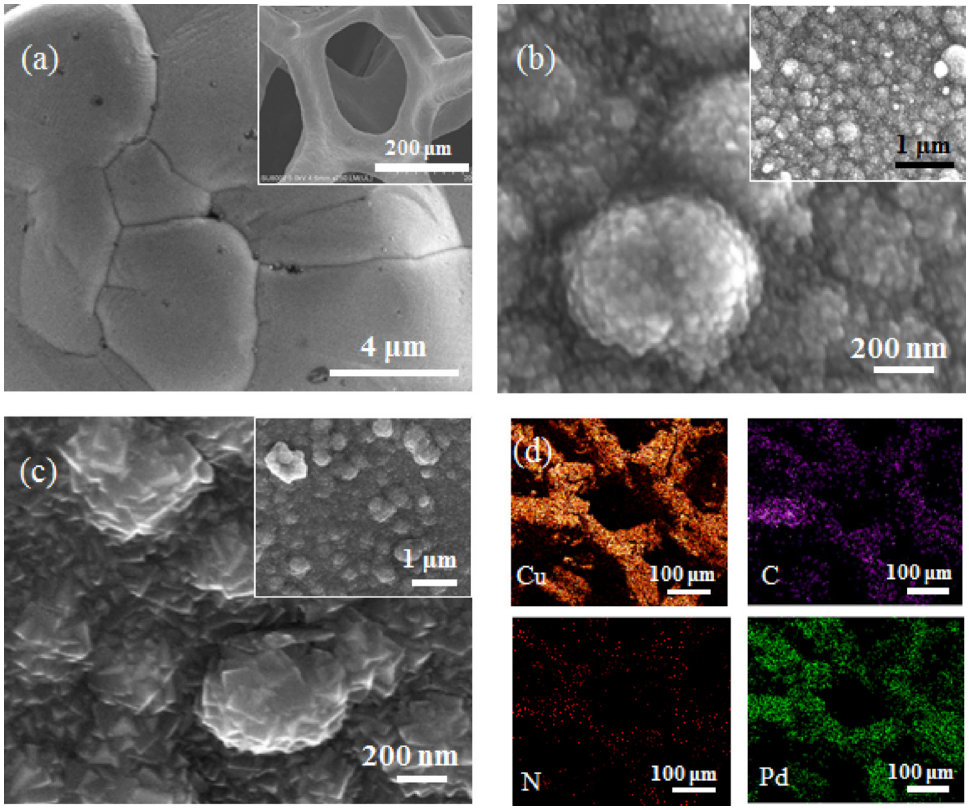

Fig. 2. SEM images of (a) Cu foam, (b) Pd/Cu foam, and (c) Pd/N-GR/Cu foam. (d) The elemental mapping images of Cu, C, N, and Pd elements of the Pd/N-GR/Cu foam.

pattern further confirms their hexagonal crystalline nature. The lattice spacing (*d*) of 0.22 nm for the Pd(111) plane can be seen on both Pd/Cu foam and Pd/N-GR/Cu foam (Fig. 3b and c). This observation is consistent with the XRD patterns (Fig. 1), indicating that the electrodeposited Pd crystal is dominated by the (111) facet. Apparently, two prominent scattering peaks at ~1365 and 1586 cm^{-1} in the Raman spectra are ascribed to the D and G bands of carbon, respectively (Fig. 3d). The former is usually induced by the topological defects in the carbon sheets, whereas the latter results from the crystalline graphitic domains [33]. The weak 2D peak at 2715 cm^{-1} proves the generation of defects in the doped N-GR sheets.

The XPS results of Cu ($2p_{3/2,\ 1/2}$) and Pd ($3d_{5/2,\ 3/2}$) suggest that both metals were present in metallic state (Fig. S1a and b). The main peak at 284.8 eV in Fig. S1c is attributed to the graphite-like sp^2 C, and the small peaks at 285.8 and 287.1 eV belong to the N-sp^2 C and N-sp^3 C bonds, respectively, which come from replacement of N atoms, defects or the edge of the graphene sheets [34]. The N1 s peak has three components centered at 398.5, 400.2, and 401.0 eV, corresponding to pyridinic-, pyrrolic-, and graphiti C—N, respectively (Fig. S1d). Such doped N atoms would cause defects such as bonding disorders and vacancies in GR lattice, and introduce a shift of the Fermi level, increasing the catalytic active sites and opening the band gap of the GR [35]. Therefore, N doping may have a significant effect on the regulation of electronic properties and improvement of electrochemical activity of GR in catalytic systems.

3.2. Performance of Pd/N-GR/Cu foam electrode for dechlorination of TCS

Fig. 4a represents the polarization curves with and without TCS at the Pd/N-GR/Cu foam electrode. In contrast to the blank electrolyte, an evident cathodic peak appears at −1.05 V when TCS is introduced into the system, and the peak current starts at around −0.58 V. It can be inferred that the peak arise from the reduction of TCS. These values are in good agreement with a previous investigation by Knust et al. [36]. The stability of the Pd/N-GR/Cu foam electrode for the catalytic TCS reduction is evidenced by the fact that the peak current varies very little (from −3.28 mA to −3.16 mA) after 50 cycles. EIS was used to analyze the kinetics of the electrochemical reactions. The arc of high frequencies represents the charge transfer resistance for cathode/electrolyte interface (Fig. 4b). The equivalent circuit model for the EIS data fitting is provided in Fig. S2, and the results are listed in Table S1. The Pd/N-GR/Cu foam electrode shows the lowest charge-transfer resistance with a R_{CT} of 2.89 Ω cm^{-2}. 3D interconnected N-GR network can offer polydimensional electron transport avenues and readily accessible active sites, and the coupling of Pd and N-GR further enhance the electrocatalytic activity which in turn results in a much faster rate of electron transfer.

The performance of various cathodes for TCS dechlorination are compared. The results in Fig. 4c reveal that the dechlorination at Pd/N-GR/Cu foam cathode proceeded much faster than at the other three cathodes. At the electrolysis time of 10 min, the dechlorination efficiency achieved 20.9%, 47.2%, 55.1%, and 93.8% for Cu foam, N-GR/Cu foam, Pd/Cu foam, and Pd/N-GR/Cu foam cathodes, respectively. The kinetics followed a pseudo first-order rate law ($R^2 > 0.982$), and the apparent rate constants (k_{ap}) are determined for the different electrodes (see Fig. 4d). For N-GR/Cu foam and Pd/Cu foam, more than 2-fold increased activities of the pristine Cu foam are achieved. Notably, Pd/N-GR/Cu foam exhibits a superior performance, and the k_{ap} is more than 5 times larger than N-GR/Cu foam and Pd/Cu foam. In addition to the active Pd sites, the 3D N-GR also play an important role in boosting the activity of the composite electrode toward TCS dechlorination. A significant synergistic effect of Pd particles and N-GR sheets in the electrocatalytic performance is clearly demonstrated.

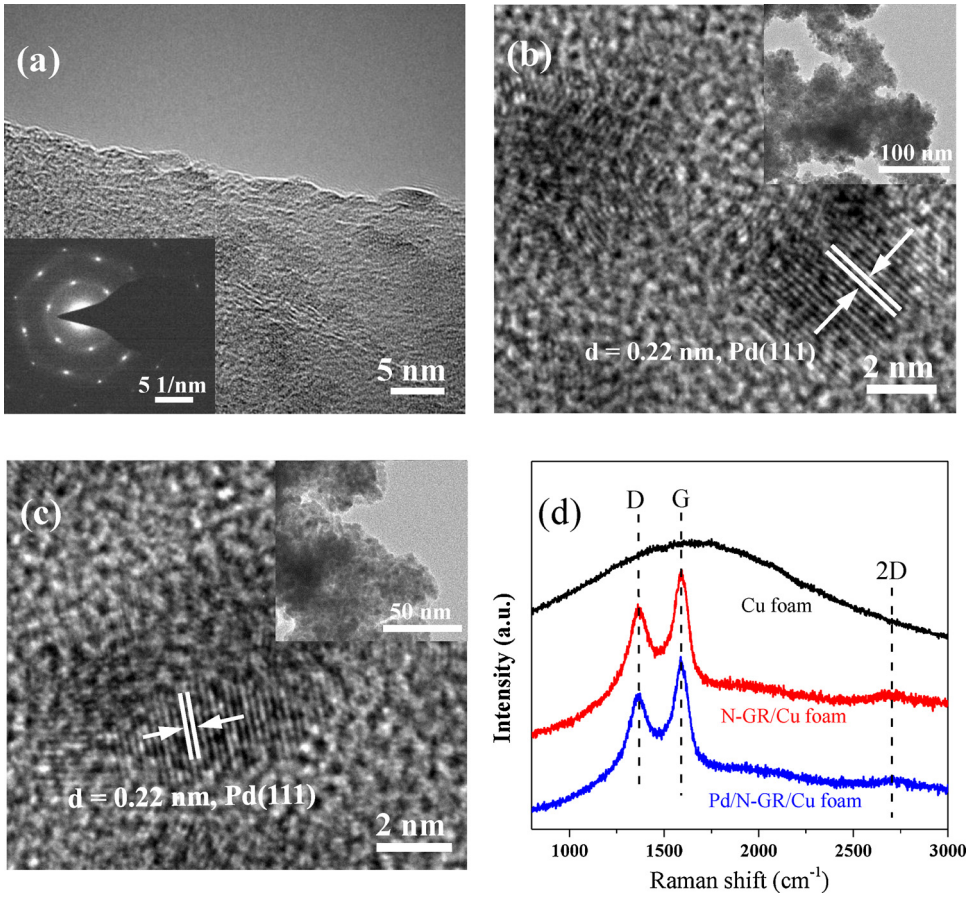

Fig. 3. (a) HRTEM image of the N-GR. The inset is corresponding SAED pattern. (b) HRTEM images of Pd particles of (b) Pd/Cu foam and (c) Pd/N-GR/Cu foam. (d) Raman spectra of Cu foam, N-GR/Cu foam, and Pd/N-GR/Cu foam.

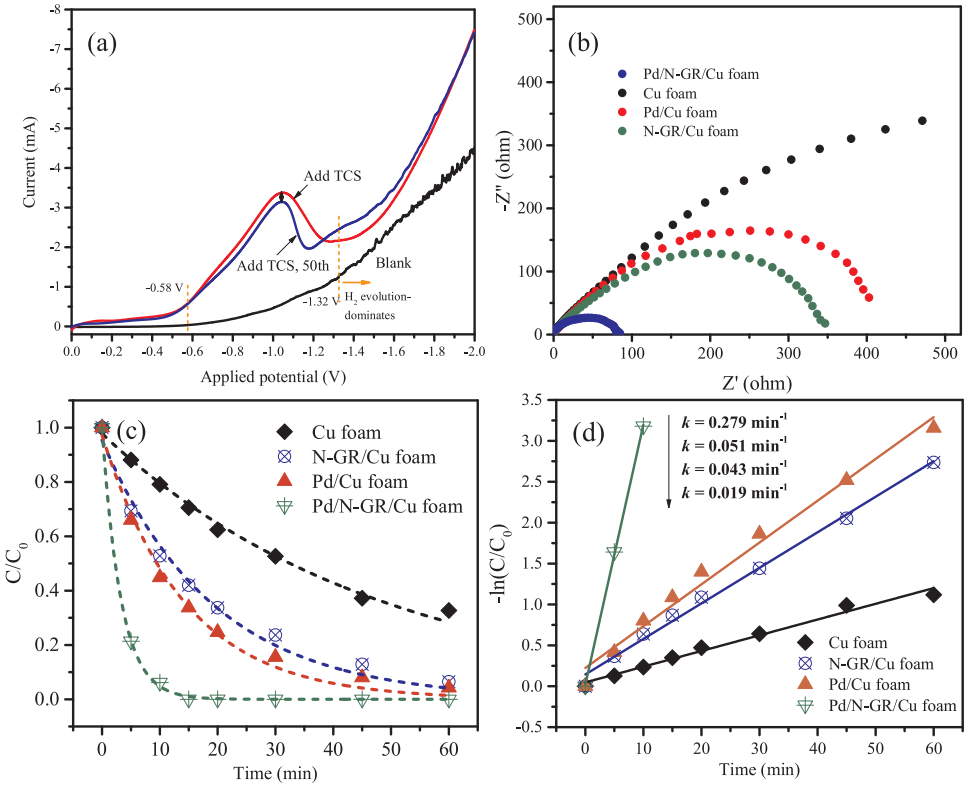

Fig. 4. (a) LSV curves of the Pd/N-GR/Cu foam electrode scanned in N_2-saturated 50 mM Na_2SO_4 solution with and without TCS. (b) Nyquist diagrams obtained at Cu foam, N-GR/Cu foam, Pd/Cu foam and Pd/N-GR/Cu foam electrodes. (c) Electrocatalytic dechlorination of TCS at different electrodes and (d) corresponding linearized pseudo first-order kinetic profiles ($[TCS]_0$ = 50 μM, applied potential = −1.2 V vs SCE, Pd loading = 0.86 mg cm^{-2}, 2 mM Na_2SO_4).

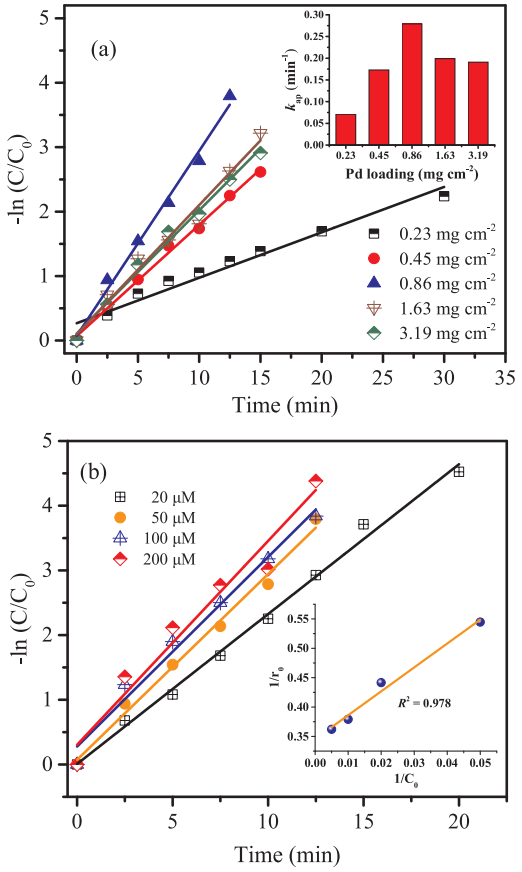

Fig. 5. (a) Influence of Pd loading on the TCS dechlorination at the Pd/N-GR/Cu foam electrode ($[TCS]_0$ = 50 μM, applied potential = −1.2 V vs SCE, 2 mM Na_2SO_4). (b) Influence of initial TCS concentration on the TCS dechlorination at the Pd/N-GR/Cu foam electrode (applied potential = −1.2 V vs SCE, Pd loading = 0.86 mg cm^{-2}, 2 mM Na_2SO_4). Inset in (b) represent the fit to the Langmuir-Hinshelwood (L-H) kinetics model.

3.3. Effect of Pd loading and initial TCS concentration

The effect of Pd loading on the TCS dechlorination at the Pd/N-GR/Cu foam electrode was investigated due to its crucial role in promoting dechlorination efficiency. As shown in Fig. 5a, upon the increase of Pd loading from 0.23 to 0.45 mg cm^{-2}, the TCS dechlorination is substantially accelerated with the rate constant increased from 0.071 to 0.173 min^{-1}. When the loading of Pd was further increased to 0.86 mg cm^{-2}, the dechlorination rate attained a maximum value of 0.279 min^{-1}, from which it began to decrease to around 0.200 min^{-1} at higher Pd loadings. Insufficient Pd loadings may not afford enough atomic H* for TCS dechlorination, thereby the efficiency can be enhanced by increasing the Pd loading within a proper range. At excessive Pd loadings, the similar inhibition of dechlorination has been reported in previous literatures, and they attributed this phenomenon to (i) the increased local currents of hydrogen evolution preventing the transfer of targets to electrode surface, and (ii) the decreased active sites due to the Pd accumulation [37,38]. In this study, high Pd loadings may lead to the block of the accessibility of TCS to the interior Pd sites, resulting in the decrease in catalytic efficiency.

The catalytic activity dependency of Pd/N-GR/Cu foam on initial TCS concentration is shown in Fig. 5b. The activity increases gradually with the initial concentration increases from 20 to 200 μM, implying that the dechlorination was controlled by the electrode surface reaction. The underlying mechanism is further clarified by fitting the experimental data to the Langmuir-Hinshelwood (L-H) model, which is widely adopted for describing the heterogeneous catalytic reaction kinetics [39]:

$$r_0 = k\theta_s = k\frac{bC_0}{1 + bC_0} \quad (1)$$

$$\frac{1}{r_0} = \frac{1}{kbC_0} + \frac{1}{k} \quad (2)$$

where r_0 is the initial reaction rate, k represents the rate constant of surface reaction, θ_s is the coverage of TCS on catalyst surface, C_0 is the initial TCS concentration, and b is the adsorption coefficient of TCS. The plot of $1/r_0$ as a function of $1/C_0$ is presented in Fig. 5b inset. A good liner relationship is observed (R^2 = 0.978), reflecting that the electrocatalytic dechlorination of TCS obeys the L-H model and the surface reaction between adsorbed TCS and reductive species is the critical step. The fitting results also show that b values are very low ($< 10^{-5}$ μM^{-1}), in accordance with the observations of inappreciable adsorption of TCS on the electrode.

3.4. Effect of cathode potential

The electrocatalytic dechlorination of TCS at the cathode potentials from −0.60 to −1.65 V at the Pd/N-GR/Cu foam electrode was investigated, and the results are presented in Fig. 6a. At −0.60 V (vs SCE), a slight decrease of TCS is observed within the 30 min reaction (~5%). The dechlorination efficiency sharply increases from 32.7% to 88.9% when the potential decreases from −0.75 to −0.90 V. The kinetic fittings clearly show the most effective potential is −1.20 V, with a dechlorination efficiency of 100% and a rate constant of 0.279 min^{-1}. Fig. 6b presents the plot of ln k_{ap} as a function of ln E (E represents the absolute value of cathode bias). From −0.60 to −1.20 V, a linear increase of ln k_{ap} with ln E is observed with the slope of 7.8 (R^2 = 0.980). This increase can be attributed to the more electrons and atomic H* provided at higher cathode potentials, which accelerates the dechlorination via both direct and indirect reduction pathway [40,41]. Nevertheless, within the cathode potentials from −1.35 to −1.65 V, a decrease in ln k_{ap} with ln E appears with a relatively slower trend (apparent rate order = −3.4). Taking into consideration that H_2 evolution has been dominated at −1.32 V (Fig. 4a), the decrement might result from the intensive H_2 production, which competes against the dechlorination in atomic H* usage (electrochemical desorption or recombination of H* to H_2 by Heyrovsky or Tafel routes) and also restrains the migration of electrons and pollutants at the electrode interface.

At various cathode potentials, the pH in the cathode cell increases from ca. 9.4 to more than 10.5 in the first 5 min and keeps nearly constant afterwards (Fig. 6c). With the decrease of the cathode potential, the equilibrium pH successively increases, although the difference is less than 0.3. It can be seen from the inset that the pH variation in each batch was almost accomplished within the first 30 s. The rapid increase during the startup period could be ascribed to the hydroxyl ions generated from the cathode, and the protons at the anode would then migrate through the solution across the proton exchange membrane, which account for the relatively constant pH afterwards [42,43].

Furthermore, an obvious decreasing trend of metal leaching upon the decrease of cathode potentials is observed (Fig. 6d). Both concentrations of released Cu^{2+} and Pd^{2+} of Pd/N-GR/Cu foam are much less than Pd/Cu foam. At the potentials more negative than −1.05 V, the concentration of Cu^{2+} is less than 0.01 mg/L, and Pd^{2+} is below the detection limit for the Pd/N-GR/Cu foam electrode, suggesting its stability during the TCS treatment. For this electrochemical reduction system, the dissolution of metals is well inhibited due to the protection by cathodic currents and alkaline conditions.

3.5. Electrocatalytic dechlorination pathway and mechanism

The intermediates for the reduction of TCS at the Pd/N-GR/Cu foam

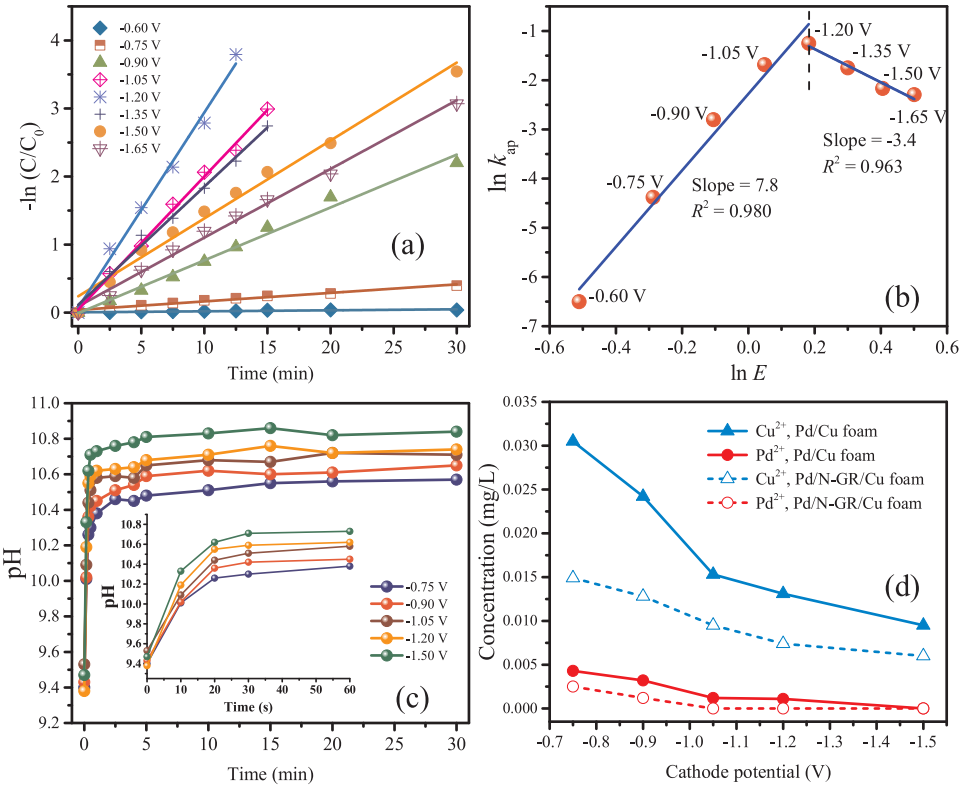

Fig. 6. (a) Pseudo-first-order representation of the electrocatalytic dechlorination of TCS at the Pd/N-GR/Cu foam electrode under different cathode potentials. (b) The relationship between ln k_{ap} and ln E. (c) Influence of cathode potential on the pH of catholyte. (d) The released Cu^{2+} and Pd^{2+} after reaction at different cathode potentials for the Pd/Cu foam and Pd/N-GR/Cu foam electrodes. $[TCS]_0$ = 50 μM, Pd loading = 0.86 mg cm^{-2}, 2 mM Na_2SO_4.

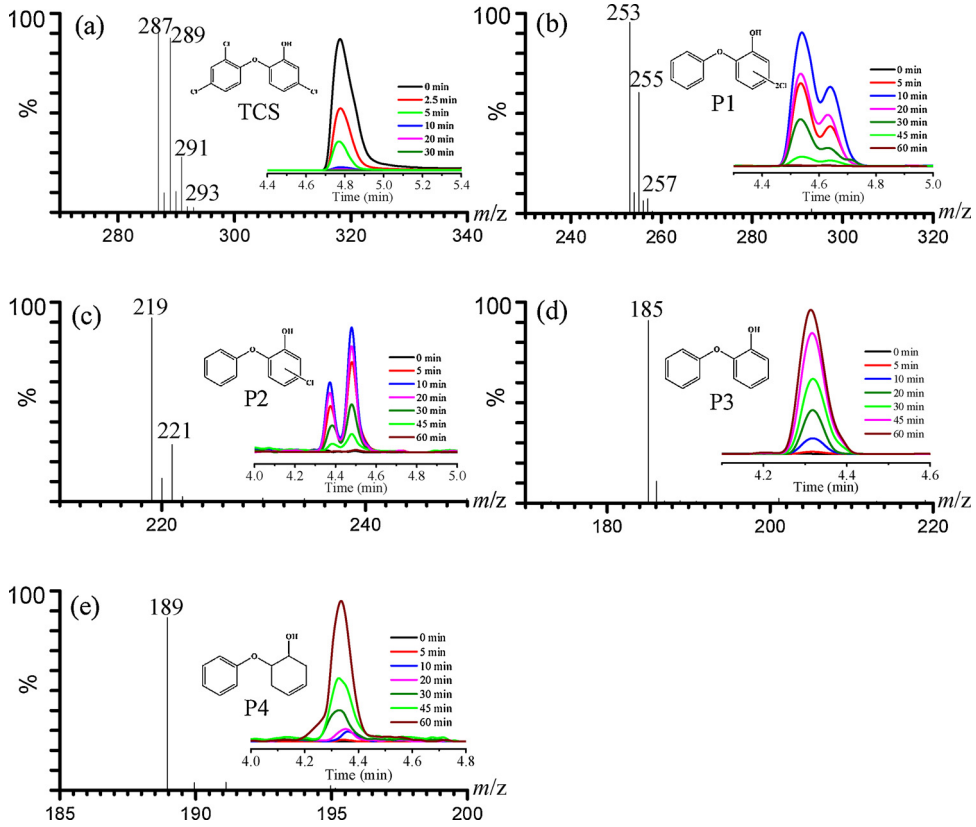

Fig. 7. The MS spectra and chromatograms of (a) TCS and (b)–(e) P1-P4 for TCS dechlorination at the Pd/N-GR/Cu foam electrode.

cathode are identified by LC-Q-TOF-MS analysis. Fig. 7 gives the MS spectra with the *m/z* values and chromatograms of the intermediates at different reaction time (0–60 min). The TCS MS spectrum before electrolysis showed an ion cluster with *m/z* 287/289/291/293, matching well with the isotopic patterns of its three chlorine atoms. The chromatographic peak of this compound disappeared gradually with the proceeding of the electrochemical reduction. Four major intermediates (P1-P4) generated during the reductive process are shown with their

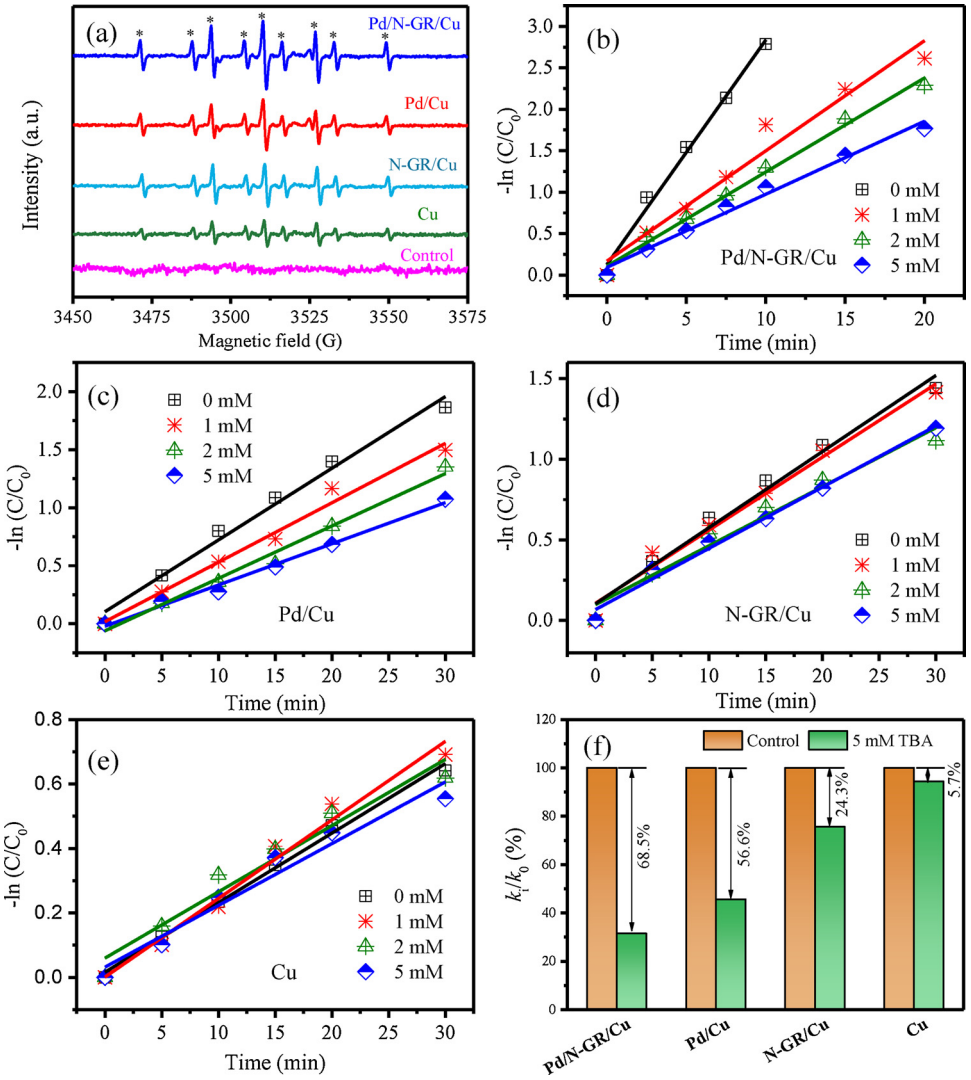

Fig. 8. (a) The DMPO spin-trapping ESR spectra at different cathodes with an applied potential of −1.2 V. (b)–(e) Linearized kinetic profiles of electrocatalytic dechlorination of TCS in different cathode systems with various TBA concentrations ($[TCS]_0$ = 50 μM, applied potential = −1.2 V vs SCE, Pd loading = 0.86 mg cm^{-2}, 2 mM Na_2SO_4). (f) Inhibition of the rate constants for TCS reduction at different cathodes.

supposed structures. The intermediate P1 was detected at *m/z* 253/255/257 with a chlorine isotope ratio of 9:6:1, indicating this compound contained two chlorines. Similarly, the fragment peaks of P2 compound at *m/z* 219/221 implied the presence of one chlorine atom as proved by the chlorine isotopic distribution. The products P1 and P2 are designated as 2-chlorinated ($C_{12}H_8Cl_2O_2$) and 1-chlorinated isomers ($C_{12}H_9ClO_2$) result from the dechlorination of TCS, respectively. Furthermore, the fragment ion at *m/z* 185 corresponds to the main final product P3, which was identified as the completely dechlorinated product 2-phenoxyphenol ($C_{12}H_{10}O_2$). It has been reported that 2-phenoxyphenol can be further hydrogenated in Pd-catalytic hydrogenation process, and the product structure was investigated by the condensed Fukui function simulation [44]. In this study, P4 was detected at *m/z* 189, which is proposed as 6-phenoxycyclohex-3-enol due to Carbons-1, 2, 5, and 6 were the most active sites for further H radical addition. The further hydrogenation or ring-opened products were not detected.

On the basis of the intermediate products analysis, the electrochemical reductive reaction pathway of TCS at the Pd/N-GR/Cu foam electrode is schemed in Fig. S3. The chromatograms show that P1 and P2 both underwent a first increase and then decrease process, while P3 was consecutively generated as the major product with a small amount of P4. Hence, it can be concluded that the electrocatalytic reduction process is very effective for the selective cleavage of the C—Cl bonds in TCS molecule. Previous literatures have pointed out that the conventional oxidative degradation of TCS generally produces highly toxic byproducts, such as 2,4-dichlorophenol, chlorophenoxyphenol, chlorodioxins and their derivatives [7,45,46]. In this work, production of these chlorinated intermediates is avoided in the selective dechlorination process. The toxicity assessment for the process will be discussed subsequently.

The direct or indirect reduction mechanism of TCS dechlorination at the different electrodes was investigated. As presented in Fig. 8a, the obvious ESR signals of DMPO-H adducts appear when applying all the four cathodes, which are absent for the black control. The peak intensities of DMPO-H at the four electrodes evolve in an order of Pd/N-GR/Cu > Pd/Cu ≈ N-GR/Cu > Cu, which indicates that the coupling of Pd and N-GR possessed a positive effect on atomic H* generation. Furthermore, *tert*-butyl alcohol (TBA), a specific quenching agent of H* [47], was used for identifying the role of atomic H* for TCS dechlorination in various cathode systems. For the Pd/N-GR/Cu foam and Pd/Cu foam, a substantially increasing inhibition of TCS removal with increased levels of TBA from 0 to 5.0 mM is observed (Fig. 8b and c). While the negative effect of TBA is not significant for the N-GR/Cu foam

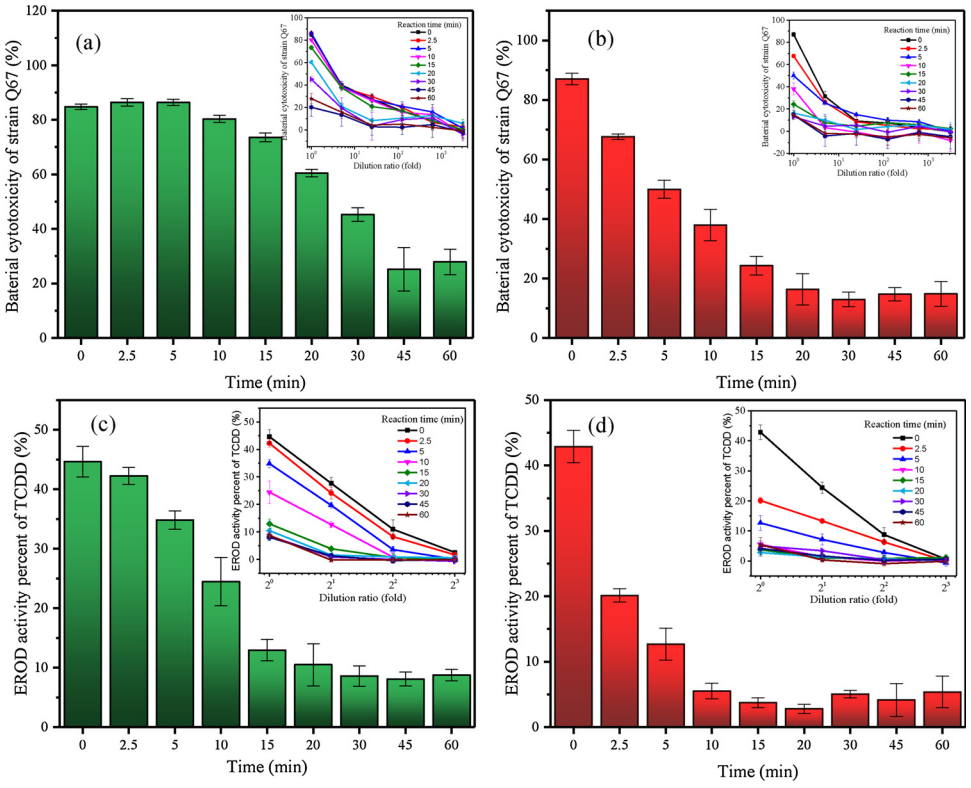

Fig. 9. Changes in bacterial cytotoxicity of reaction solutions during the electrochemical reduction process at (a) Pd/Cu foam and (b) Pd/N-GR/Cu foam electrodes. Changes in AhR activity of reaction solutions at (c) Pd/Cu foam and (d) Pd/N-GR/Cu foam electrodes. $[TCS]_0$ = 250 μM, applied potential = −1.2 V vs SCE, Pd loading = 0.86 mg cm^{-2}, 2 mM Na_2SO_4. The insets show the dose-response curves for the samples at different reaction time. Error bars represent standard deviations (n = 3). AhR activity is expressed as percentage of the maximum response that is observed for the 2,3,7,8-tetrachlorodibenzo-*p*-dioxin standard (%-TCDD-max).

and Cu foam electrodes (Fig. 8d and e). From the rate constant ratio (the ratio of that in the presence of TBA to the original one without TBA) in Fig. 8f, the contribution of atomic H* to the TCS removal follows the order of Pd/N-GR/Cu (68.5%) > Pd/Cu (56.6%) > N-GR/Cu (24.3%) > Cu (5.7%).

According to the hydrogen evolution reaction (HER) mechanism, atomic H* can be first produced by Volmer reaction, thereby the DMPO-H peaks were detected at the four cathodes. Atomic H* can be stockpiled in the Pd particles and further be utilized for the H*-mediated hydrogenation process [48,49], and thus are responsible for TCS dechlorination at the Pd-loaded electrodes. The higher contribution of H* at the Pd/N-GR/Cu foam in contrast to the Pd/Cu foam can be ascribed to the improved electronic properties of the 3D N-GR sheets, which boost the electric conductivity through the electrode and accelerate the H* generation. Although N-GR was reported to be a catalyst for hydrogen dissociative adsorption, it is inferior to Pd in either H* uptake capacity or subsequent H* migration [50,51]. So, for N-GR/Cu foam, the role of atomic H* is relatively minor for TCS dechlorination. Cu is catalytically inert to the H* storage and immobilization, and they would combine to form H_2 rapidly via Heyrovsky or Tafel avenues under the applied electric field [52], which drives surface reactions to favor direct reduction by the electrons.

3.6. Toxicity assessment for electrochemical reduction treatment

The evolution of toxicity of TCS solution during electrochemical reduction treatment was evaluated by two kinds of in vitro bioassays including acute toxicity in luminescent bacteria (*Vibrio qinghaiensis* sp. *Nov.*, strain Q67) and AhR activity by H4IIE-EROD assay. Strain Q67 is a sensitive model for assessing acute toxicity of chemicals and water quality [53]. As shown in Fig. 9a, for the Pd/Cu foam electrode, the luminescence inhibition ratio was 84.8 ± 1.0% at the initial TCS concentration (0 min). Then the bacterial cytotoxicity of the solution slowly decreased to 73.6 ± 1.6% and 27.9 ± 4.7% at 15 and 60 min, respectively. In contrast, the bacterial cytotoxicity at Pd/N-GR/Cu foam electrode decreased much faster from 87.1 ± 1.9% to 24.3 ± 3.2% and 14.8 ± 4.1% at 15 and 60 min, respectively (Fig. 9b).

The results of EROD assay of AhR activity are given in Fig. 9c and d. AhR is a ligand-dependent transcription factor mediating a variety of toxicological and biological effects from exposure to numerous chemicals [54]. The EROD assay is often used to investigate the AhR-dependent, dioxin-like effects induced by halogenated aromatic compounds, like polychlorinated naphthalene, polychlorinated biphenyl, and polychlorinated dibenzo-*p*-dioxins and -furans [55,56]. TCS is not only structure similar to these compounds but also an AhR agonist [57]. The maximum AhR activities observed for the untreated TCS solutions in the two batches are 44.6 ± 2.6% and 42.9 ± 2.5%, respectively, which are close to 40.6 ± 6.1% of a similar TCS concentration reported in the literature [56]. For EROD assay, the variation trend was analogous to that of acute toxicity. The AhR activity of reaction solutions decreased to 12.9 ± 1.8% and 8.8 ± 1.0% at 15 and 60 min for the Pd/Cu foam. For the Pd/N-GR/Cu foam, the decrease of AhR activity proceeds more rapidly, and the activities are all below 5.3 ± 2.4% after 15 min electrolysis, indicating a very low potency for AhR induction after electrocatalytic dechlorination. The insets illustrate the potency of TCS solution decreased in a dose-response dependent manner, which clearly demonstrated that the intermediates concentration is correlative with bacterial cytotoxicity and AhR activity.

The probable mechanism for bacterial cytotoxicity induced by TCS in strain Q67 is that TCS can block synthesis of fatty acids in bacteria through inhibition of enoyl reductase, and the chlorine groups on TCS play a key role for the binding between enoyl reductase and TCS [57,58]. Meanwhile, previous studies also showed a positive correlation between degree of chlorination of compound and AhR mediated activity, like PCNs and some chlorinated polycyclic aromatic hydrocarbons, and proved that AhR agonists with lower level of chloride could significantly decrease the AhR activity when comparing with their high chlorinated derivatives [59,60]. As discussed above, the electrochemical reduction of TCS could effectively break the C-Cl bonds, thus significantly reduce both bacterial cytotoxicity and AhR activity. The findings in this study provide a systematic understanding on the enhanced reactivity by coupling of Pd and N-GR for the

electrochemical reduction, and demonstrate that the reductive transformation of TCS could be a promising method to mitigate its toxic effects.

4. Conclusions

The Pd/N-GR/Cu foam electrode was successfully synthesized by a CVD method, followed by electrodepositing Pd particles. The N-GR presents a typical hexagonal crystalline structure, while Pd crystal is dominated by the (111) facet. The pyridinic- and pyrroli C—N are the dominant N species. Coupling of Pd and N-GR resulted in enhanced electronic properties, and a significant synergistic effect was displayed for the electrocatalytic reduction of TCS. Increase of Pd loading could accelerate the TCS dechlorination, while at high Pd loadings the dechlorination was inhibited. The ln k_{ap} rose linearly with ln E from -0.60 to -1.20 V ($R^2 = 0.980$), and then turned to decrease at more negative potentials due to the increased currents of hydrogen evolution. The major final product of electrochemical reduction was the completely dechlorinated product 2-phenoxyphenol. Atomic H*-mediated indirect reduction was responsible for the C—Cl bonds breakage. Toxicity tests including acute toxicity and EROD assay reveal that the treatment by electrochemical reduction largely reduces the bacterial cytotoxicity and AhR activity of TCS solution. In conclusion, the Pd/N-GR/Cu foam electrode may potentially serve as an ideal candidate for electrocatalytic dechlorination in HOCs treatments.

Acknowledgments

This work was supported by the National Natural Science Foundation of China (51808535) and Beijing Natural Science Foundation (8184088).

Appendix A. Supplementary data

Supplementary material related to this article can be found, in the online version, at doi:https://doi.org/10.1016/j.apcatb.2018.09.013.

References

[1] L.M. McMurry, M. Oethinger, S.B. Levy, Triclosan targets lipid synthesis, Nature 394 (1998) 531–532.
[2] J.A. Ruszkiewicz, S. Li, M. Aschner, Is triclosan a neurotoxic agent? J. Toxicol. Environ. Health B Crit. Rev. 20 (2017) 104–117.
[3] H. Singer, S. Muller, C. Tixier, L. Pillonel, Triclosan: occurrence and fate of a widely used biocide in the aquatic environment: field measurements in wastewater treatment plants, surface waters, and lake sediments, Environ. Sci. Technol. 36 (2002) 4998–5004.
[4] R. Oliveira, I. Domingues, C. Koppe Grisolia, A.M. Soares, Effects of triclosan on zebrafish early-life stages and adults, Environ. Sci. Pollut. Res. 16 (2009) 679–688.
[5] N. Veldhoen, R.C. Skirrow, H. Osachoff, H. Wigmore, D.J. Clapson, M.P. Gunderson, G. Van Aggelen, C.C. Helbing, The bactericidal agent triclosan modulates thyroid hormone-associated gene expression and disrupts postembryonic anuran development, Aquat. Toxicol. 80 (2006) 217–227.
[6] J.M. Buth, M. Grandbois, P.J. Vikesland, K. McNeill, W.A. Arnold, Aquatic photochemistry of chlorinated triclosan derivatives: potential source of polychlorodibenzo-p-dioxins, Environ. Toxicol. Chem. 28 (2009) 2555–2563.
[7] J. Chen, R. Qu, X. Pan, Z. Wang, Oxidative degradation of triclosan by potassium permanganate: kinetics, degradation products, reaction mechanism, and toxicity evaluation, Water Res. 103 (2016) 215–223.
[8] H. Gao, J. Chen, Y. Zhang, X. Zhou, Sulfate radicals induced degradation of Triclosan in thermally activated persulfate system, Chem. Eng. J. 306 (2016) 522–530.
[9] A. Ogutverici, L. Yilmaz, U. Yetis, F.B. Dilek, Triclosan removal by NF from a real drinking water source-effect of natural organic matter, Chem. Eng. J. 283 (2016) 330–337.
[10] J. Peng, H. Shi, J. Li, L. Wang, Z. Wang, S. Gao, Bicarbonate enhanced removal of triclosan by copper(II) catalyzed Fenton-like reaction in aqueous solution, Chem. Eng. J. 306 (2016) 484–491.
[11] S. Suarez, M.C. Dodd, F. Omil, U.V. Gunten, Kinetics of triclosan oxidation by aqueous ozone and consequent loss of antibacterial activity: relevance to municipal wastewater ozonation, Water Res. 41 (2007) 2481–2490.
[12] M.A. Oturan, J.J. Aaron, Advanced oxidation processes in water/wastewater treatment: principles and applications. A review, Crit. Rev. Environ. Sci. Technol. 44 (2014) 2577–2641.
[13] E. Brillas, I. Sirés, M.A. Oturan, Electro-Fenton process and related electrochemical technologies based on Fenton's reaction chemistry, Chem. Rev. 109 (2009) 6570–6631.
[14] I. Sirés, N. Oturan, M.A. Oturan, R.M. Rodríguez, J.A. Garrido, E. Brillas, Electro-Fenton degradation of antimicrobials triclosan and triclocarban, Electrochim. Acta 52 (2007) 5493–5503.
[15] J. Wang, J. Farrell, Electrochemical inactivation of triclosan with boron doped diamond film electrodes, Environ. Sci. Technol. 38 (2004) 5232–5237.
[16] J. Radjenovic, M.J. Farre, Y. Mu, W. Gernjak, J. Keller, Reductive electrochemical remediation of emerging and regulated disinfection byproducts, Water Res. 46 (2012) 1705–1714.
[17] C.Y. Cui, X. Quan, H.T. Yu, Y.H. Han, Electrocatalytic hydrodehalogenation of pentachlorophenol at palladized multiwalled carbon nanotubes electrode, Appl. Catal. B: Environ. 80 (2008) 122–128.
[18] B. Yang, G. Yu, J. Huang, Electrocatalytic hydrodechlorination of 2,4,5-trichlorobiphenel on a palladium-modified nickel foam cathode, Environ. Sci. Technol. 41 (2007) 7503–7508.
[19] J. Radjenovic, D.L. Sedlak, Challenges and opportunities for electrochemical processes as next-generation technologies for the treatment of contaminated water, Environ. Sci. Technol. 49 (2015) 11292–11302.
[20] C. Durante, A.A. Isse, G. Sandonà, A. Gennaro, Electrochemical hydrodehalogenation of polychloromethanes at silver and carbon electrodes, Appl. Catal. B: Environ. 88 (2009) 479–489.
[21] L.Z. Huang, S.U. Pedersen, E.T. Bjerglund, P. Lamagni, M. Glasius, H.C.B. Hansen, K. Daasbjerg, Hierarchical MoS_2 nanosheets on flexible carbon felt as an efficient flow-through electrode for dechlorination, Environ. Sci. Nano 4 (2017) 2286–2296.
[22] T. Li, J. Farrell, Reductive dechlorination of trichloroethene and carbon tetrachloride using iron and palladized-iron cathodes, Environ. Sci. Technol. 34 (2000) 173–179.
[23] J.Y. Lee, J.G. Lee, S.H. Lee, M. Seo, L. Piao, J.H. Bae, S.Y. Lim, Y.J. Park, T.D. Chung, Hydrogen-atom-mediated electrochemistry, Nat. Commun. 4 (2013) 2766–2733.
[24] G. Jiang, M. Lan, Z. Zhang, X. Lv, Z. Lou, X. Xu, F. Dong, S. Zhang, Identification of active hydrogen species on palladium nanoparticles for an enhanced electrocatalytic hydrodechlorination of 2, 4-dichlorophenol in water, Environ. Sci. Technol. 51 (2017) 7599–7605.
[25] S. Yuan, X. Mao, A.N. Alshawabkeh, Efficient degradation of TCE in groundwater using Pd and electro-generated H_2 and O_2: a shift in pathway from hydrodechlorination to oxidation in the presence of ferrous ions, Environ. Sci. Technol. 46 (2012) 3398–3405.
[26] M.M. Liu, R.Z. Zhang, W. Chen, Graphene-supported nanoelectrocatalysts for fuel cells: synthesis, properties, and applications, Chem. Rev. 114 (2014) 117–5160.
[27] X.R. Wang, X.L. Li, L. Zhang, Y. Yoon, P.K. Weber, H.L. Wang, J. Guo, H.J. Dai, N-doping of graphene through electrothermal reactions with ammonia, Science 324 (2009) 768–771.
[28] S. Kabir, A. Serov, K. Artyushkova, P. Atanassov, Nitrogen-doped three-dimensional graphene-supported palladium nanocomposites: high-performance cathode catalysts for oxygen reduction reactions, ACS Catal. 7 (2017) 6609–6618.
[29] V.B. Parambhath, R. Nagar, K. Sethupathi, S. Ramaprabhu, Investigation of spillover mechanism in palladium decorated hydrogen exfoliated functionalized graphene, J. Phys. Chem. C 115 (2011) 15679–15685.
[30] B.P. Vinayan, R. Nagar, N. Rajalakshmi, S. Ramaprabhu, Novel platinum-cobalt alloy nanoparticles dispersed on nitrogen-doped graphene as a cathode electrocatalyst for PEMFC applications, Adv. Funct. Mater. 22 (2012) 3519–3526.
[31] L. Zhao, S. Li, J. He, G. Tian, Q. Wei, H. Li, Enzyme-free electrochemical immunosensor configured with Au-Pd nanocrystals and N-doped graphene sheets for sensitive detection of AFP, Biosens. Bioelectron. 49 (2013) 222–225.
[32] R. Mao, X. Zhao, H.C. Lan, H.J. Liu, J.H. Qu, Efficient electrochemical reduction of bromate by a Pd/rGO/CFP electrode with low applied potentials, Appl. Catal. B: Environ. 160–161 (2014) 179–187.
[33] X. Zhang, J. Zhu, C.S. Tiwary, Z. Ma, H. Huang, J. Zhang, Z. Lu, W. Huang, Y. Wu, Palladium nanoparticles supported on nitrogen and sulfur dual-doped graphene as highly active electrocatalysts for formic acid and methanol oxidation, ACS Appl. Mater. Interfaces 8 (2016) 10858–10865.
[34] D.C. Wei, Y.Q. Liu, Y. Wang, H.L. Zhang, L.P. Huang, G. Yu, Synthesis of N-doped graphene by chemical vapor deposition and its electrical properties, Nano Lett. 9 (2009) 1752–1758.
[35] L. Liu, S.M. Ryu, M.R. Tomasik, E. Stolyarova, N. Jung, M.S. Hybertsen, M.L. Steigerwald, L.E. Brus, G.W. Flynn, Graphene oxidation: thickness-dependent etching and strong chemical doping, Nano Lett. 8 (2008) 1965–1970.
[36] K.N. Knust, M.P. Foley, M.S. Mubarak, S. Skljarevski, K. Raghavachari, D.G. Peters, Electrochemical reduction of 5-chloro-2-(2, 4-dichlorophenoxy) phenol (triclosan) in dimethylformamide, J. Electroanal. Chem. 638 (2010) 100–108.
[37] M.O. Nutt, J.B. Hughes, M.S. Wong, Designing Pd-on-Au bimetallic nanoparticle catalysts for trichloroethene hydrodechlorination, Environ. Sci. Technol. 39 (2005) 1346–1353.
[38] Y. Wu, L. Gan, S. Zhang, B. Jiang, H. Song, W. Li, Y. Pan, A. Li, Enhanced electrocatalytic dechlorination of para-chloronitrobenzene based on Ni/Pd foam electrode, Chem. Eng. J. 316 (2017) 146–153.
[39] Z.M. De Pedro, J.A. Casas, L.M. Gomez-Sainero, J.J. Rodriguez, Hydrodechlorination of dichloromethane with a Pd/AC catalyst: reaction pathway and kinetics, Appl. Catal. B: Environ. 98 (2010) 79–85.
[40] R. Mao, N. Li, H.C. Lan, X. Zhao, H.J. Liu, J.H. Qu, M. Sun, Dechlorination of trichloroacetic acid using a noble metal-free graphene-Cu foam electrode via direct cathodic reduction and atomic H*, Environ. Sci. Technol. 50 (2016) 3829–3837.
[41] C. Liu, A.Y. Zhang, D.N. Pei, H.Q. Yu, Efficient electrochemical reduction of

nitrobenzene by defect engineered TiO_{2-x} single crystals, Environ. Sci. Technol. 50 (2016) 5234–5242.
[42] G.C. Gil, I.S. Chang, B.H. Kim, M. Kim, J.K. Jang, H.S. Park, H.J. Kim, Operational parameters affecting the performance of a mediator-less microbial fuel cell, Biosens. Bioelectron. 18 (2003) 327–334.
[43] R.A. Rozendal, H.V.M. Hamelers, C.J.N. Buisman, Effects of membrane cation transport on pH and microbial fuel cell performance, Environ. Sci. Technol. 40 (2006) 5206–5211.
[44] B. Han, W. Liu, J. Li, J. Wang, D. Zhao, R. Xu, Z. Lin, Catalytic hydrodechlorination of triclosan using a new class of anion-exchange-resin supported palladium catalysts, Water Res. 120 (2017) 199–210.
[45] D.E. Latch, J.L. Packer, B.L. Stender, J. VanOverbeke, W.A. Arnold, K. McNeill, Aqueous photochemistry of triclosan: formation of 2,4-dichlorophenol, 2,8-dichlorodibenzo-p-dioxin, and oligomerization products, Environ. Toxicol. Chem. 24 (2005) 517–525.
[46] K.L. Rule, V.R. Ebbett, P.J. Vikesland, Formation of chloroform and chlorinated organics by free-chlorine-mediated oxidation of triclosan, Environ. Sci. Technol. 39 (2005) 3176–3185.
[47] S.P. Mezyk, W.J. Cooper, K.P. Madden, D.M. Bartels, Free radical destruction of N-nitrosodimethylamine in water, Environ. Sci. Technol. 38 (2004) 3161–3167.
[48] B.P. Chaplin, M. Reinhard, W.F. Schneider, C. Schüth, J.R. Shapley, T.J. Strathmann, C.J. Werth, Critical review of Pd-based catalytic treatment of priority contaminants in water, Environ. Sci. Technol. 46 (2012) 11469–11470.
[49] W.C. Conner, J.L. Falconer, Spillover in heterogeneous catalysis, Chem. Rev. 95 (1995) 759–788.
[50] Z.M. Ao, A.D. Hernandez-Nieves, F.M. Peeters, S. Li, The electric field as a novel switch for uptake/release of hydrogen for storage in nitrogen doped grapheme, Phys. Chem. Chem. Phys. 14 (2012) 1463–1467.
[51] V.B. Parambhath, R. Nagar, S. Ramaprabhu, Effect of nitrogen doping on hydrogen storage capacity of palladium decorated grapheme, Langmuir 28 (2012) 7826–7833.
[52] L.E. Knitt, J.R. Shapley, T.J. Strathmann, Rapid metal-catalyzed hydrodehalogenation of iodinated X-ray contrast media, Environ. Sci. Technol. 42 (2008) 577–583.
[53] M. Ma, Z. Tong, Z. Wang, W. Zhu, Acute toxicity bioassay using the freshwater luminescent bacterium Vibrio-qinghaiensis sp. Nov.-Q67, Bull. Environ. Contam. Toxicol. 62 (1999) 247–253.
[54] M.S. Denison, A.A. Soshilov, G. He, D.E. DeGroot, B. Zhao, Exactly the same but different: promiscuity and diversity in the molecular mechanisms of action of the aryl hydrocarbon (dioxin) receptor, Toxicol. Sci. 124 (2011) 1–22.
[55] T. Tsutsumi, Y. Amakura, M. Nakamura, D. Brown, G.C. Clark, K. Sasaki, M. Toyoda, T. Maitani, Validation of the CALUX bioassay for the screening of PCDD/Fs and dioxin-like PCBs in retail fish, Analyst 128 (2003) 486–492.
[56] D. Villeneuve, K. Kannan, J. Khim, J. Falandysz, V. Nikiforov, A. Blankenship, J. Giesy, Relative potencies of individual polychlorinated naphthalenes to induce dioxin-like responses in fish and mammalian in vitro bioassays, Arch. Environ. Contam. Toxicol. 39 (2000) 273–281.
[57] A.B. Dann, A. Hontela, Triclosan: environmental exposure, toxicity and mechanisms of action, J. Appl. Toxicol. 31 (2011) 285–311.
[58] R.J. Heath, J.R. Rubin, D.R. Holland, E. Zhang, M.E. Snow, C.O. Rock, Mechanism of triclosan inhibition of bacterial fatty acid synthesis, J. Biol. Chem. 274 (1999) 11110–11114.
[59] Y. Horii, J.S. Khim, E. Higley, J.P. Giesy, T. Ohura, K. Kannan, Relative potencies of individual chlorinated and brominated polycyclic aromatic hydrocarbons for induction of aryl hydrocarbon receptor-mediated responses, Environ. Sci. Technol. 43 (2009) 2159–2165.
[60] T. Ohura, M. Morita, M. Makino, T. Amagai, K. Shimoi, Aryl hydrocarbon receptor-mediated effects of chlorinated polycyclic aromatic hydrocarbons, Chem. Res. Toxicol. 20 (2007) 1237–1241.